Buckling analysis of thin-walled functionally graded sandwich box beams

Domagoj Lanc[a,*], Thuc P. Vo[b], Goran Turkalj[a], Jaehong Lee[c]

[a]*Department of Engineering Mechanics, Faculty of Engineering, University of Rijeka, Vukovarska 58, HR-51000 Rijeka, Croatia.*
[b]*Faculty of Engineering and Environment, Northumbria University, Newcastle upon Tyne, NE1 8ST, UK.*
[c]*Department of Architectural Engineering, Sejong University 98 Kunja Dong, Kwangjin Ku, Seoul 143-747, Korea.*

Abstract

Buckling analysis of thin-walled functionally graded (FG) sandwich box beams is investigated. Material properties of the beam are assumed to be graded through the wall thickness. The Euler-Bernoully beam theory for bending and the Vlasov theory for torsion are applied. The non-linear stability analysis is performed in framework of updated Lagrangian formulation. In order to insure the geometric potential of semitangental type for internal bending and torsion moments, the non-linear displacement field of thin-walled cross-section is adopted. Numerical results are obtained for FG sandwich box beams with simply-supported, clamped-free and clamped-clamped boundary conditions to investigate effects of the power-law index and skin-core-skin thickness ratios on the critical buckling loads and post-buckling respones. Numerical results show that the above-mentioned effects play very important role on the buckling analysis of sandwich box beams.

Keywords: FG sandwich box beams; Buckling; Finite element

1. Introduction

In recent years, there is a rapid increase in the use of functionally graded (FG) structures. Thin-walled FG beams have practical interest and future potential particularly in aerospace and mechanical applications due to high strength-to-weight ratio. Many papers have been devoted to study bending, vibration and buckling of FG and FG sandwich beams and only some of them are cited here [1-13]. In these papers, different theories (classical beam theory, first-order beam theory and higher-order beam theory) and various material distribution laws of FG beams have been introduced. However, there are quite a few papers which mainly

* Corresponding author
Email address: dlanc@riteh.hr (Domagoj Lanc)

studied dynamics of FG thin-walled box beams. Librescu et al. [14] studied instability, vibration analysis along with the effects of temperature gradients and volume fraction of FG thin-walled beams. Piovan and Machado [15] adopted a second-order nonlinear displacement field in order to study the dynamic stability of simply-supported FG box beams under an axial external force. Based on the first-order shear deformation theory, Ziane et al. [16] investigated the free vibration of FG box beams by using theformulation of an exact dynamic stiffness matrix. Carvalho et al. [17] studied the nonlinear nonplanar vibration of a clamped-free slender FG box beam. Mashat et al. [18] used Carrera Unified Formulation to perform vibration of thin- and thick-walled FG box beams.

In this paper, which is an extension of previous work [19], buckling analysis of FG sandwich box beams is presented. Material properties of the beam are assumed to be graded across the wall thickness.

The model is based on assumptions of large displacements but small strains, the Euler-Bernoully beam theory for bending and the Vlasov theory for torsion. The thin-walled beam members are supposed to be straight and prismatic. External loads are assumed to be static and conservative. In order to perform non-linear stability analysis in load deflection manner, the updated Lagrangian (UL) incremental descriptions is applied. The non-linear cross section displacement field which accounts for the second order displacement terms due to large rotations is implemented. The generalized displacement control method is employed in terms of the incremental-iterative solution scheme. Updating of nodal orientations at the end of the each iteration is performed using the transformation rule which applies for semitangental incremental rotations, while the force recovering is performed according to the conventional approach (CA).

Numerical results are obtained for sandwich box beams with simply-supported, clamped free and clamped-clamped boundary conditions to investigate effects of the power-law index and skin-core-skin thickness ratios on the critical buckling loads and post-buckling respones. Numerical results show that the abovementioned effects play very important role on the buckling analysis of sandwich box beams.

2. Basic consideration

To derive the finite element model of a thin-walled FG box beam, the following assumptions are made:

1. The contour of the thin wall does not deform in its own plane.

2. The linear shear strain $\bar{\gamma}_{zs}$ of the middle surface is to have the same distribution in the contour direction as it does in the St. Venant torsion in each element.

3. The bending shear deformation are neglected.

4. The local buckling as well as the distortional buckling are not considered.

2.1. Beam kinematics

In this paper, two sets of coordinate systems, which are mutually interrelated, are used. The first coordinate system is Cartesian coordinate system (z, x, y), for which z-axis coincides with the beam axis passing through the centroid O of each cross-section, while the x- and y-axes are the principal inertial axes of the cross-section taken along the width and height of the beam. The second coordinate system is contour coordinate (z, n, s) as shown in Fig. 1, wherein coordinate z coincident with beam z-axis, the coordinate s is measured along the tangent of the middle surface in a counter-clockwise direction, while n is the coordinate perpendicular to s. Incremental displacement measures of a cross-section are defined as

$$\begin{aligned} &w_o = w_o(z), u_o = u_o(z), v_o = v_o(z), \varphi_z = \varphi_z(z), \\ &\varphi_x = -v_o' = \varphi_x(z),\ \varphi_y = u_o' = \varphi_z(z), \theta = -\varphi_z' = \theta(z) \end{aligned} \tag{1}$$

where w_o, u_o and v_o are the rigid-body translations of the cross-section associated with the centroid in the z-, x- and y-directions, respectively; φ_z, φ_x and φ_y are the rigid-body rotations about the z-, x- and y-axis, respectively; θ is a parameter defining the warping of the cross-section. The superscript 'prime' indicates the derivative with respect to z.

If rotations are small, the incremental displacement field of a thin-walled cross-section contains only the first-order displacement terms [20]:

$$\begin{aligned} &u_z = w_o - y\, v_o' - x\ u_o' - \omega\varphi_z', \\ &u_x = u_o - y\,\varphi_z, \\ &u_y = v_o + x\,\varphi_z \end{aligned} \tag{2}$$

in which u_z, u_x and u_y are the linear or first-order displacement increments of an arbitrary point on the cross-section defined by the position coordinates x and y and the warping function $\omega(x, y)$. If the assumption of small rotations is not invalid, then the second-order displacement increments:

$$\begin{aligned} &\tilde{u}_z = 0.5\left[\ \varphi_z\varphi_x x + \varphi_z\varphi_y y\right], \\ &\tilde{u}_x = 0.5\left[\varphi_x\varphi_y y - \left(\varphi_z^2 + \varphi_y^2\right)x\right], \\ &\tilde{u}_y = 0.5\left[\varphi_x\varphi_y x - \left(\varphi_z^2 + \varphi_x^2\right)y\right] \end{aligned} \tag{3}$$

due to large rotations should be added to those from Eq. (2).

The strain tensor components, corresponding to nonlinear displacement field, are:

$$\varepsilon_{ij}=\frac{1}{2}\left[\left(u_i+\tilde{u}_i\right)_{,j}+\left(u_j+\tilde{u}_j\right)_{,i}+\left(u_k+\tilde{u}_k\right)_{,i}\left(u_k+\tilde{u}_k\right)_{,j}\right]\cong e_{ij}+\eta_{ij}+\tilde{e}_{ij} \tag{4}$$

$$2e_{ij}=u_{i,j}+u_{j,i},\qquad 2\eta_{ij}=u_{k,i}u_{k,j},\qquad 2\tilde{e}_{ij}=\tilde{u}_{i,j}+\tilde{u}_{j,i} \tag{5}$$

The last term $\tilde{e}_{ij}$ contains the second-order displacements due to the large rotations.

2.2. Contour displacements

The contour mid-line displacements are $\bar{w},\bar{u},\bar{v}$, while the out of mid-line displacement components are defined as:

$$w(z,s,n)=\bar{w}-n\frac{\partial\bar{u}}{\partial z};\qquad v(z,s,n)=\bar{v}-n\frac{\partial\bar{u}}{\partial s};\qquad u(z,s,n)=\bar{u}\quad . \tag{6}$$

Beam to contour displacement relation can be given as:

$$\begin{aligned}&\bar{w}^L=u_z(z,s,n),\quad \bar{w}^{NL}=\tilde{u}_z(z,s,n);\\&\bar{v}^L=u_x(z,s,n)\cos\beta+u_y(z,s,n)\sin\beta,\quad \bar{v}^{NL}=\tilde{u}_x(z,s,n)\cos\beta+\tilde{u}_y(z,s,n)\sin\beta;\\&\bar{u}^L=u_x(z,s,n)\sin\beta-u_y(z,s,n)\cos\beta,\quad \bar{u}^{NL}=\tilde{u}_x(z,s,n)\sin\beta-\tilde{u}_y(z,s,n)\cos\beta\end{aligned} \tag{7}$$

where indexes *L* and *NL* indicates linear and nonlinear parts respectively.

Out of mid-line displacements can also be separate into linear and non-linear components:

$$w^L(z,s,n)=\bar{w}^L-n\frac{\partial\bar{u}^L}{\partial z};\qquad v^L(z,s,n)=\bar{v}^L-n\frac{\partial\bar{u}^L}{\partial s};\qquad u^L(z,s,n)=\bar{u}^L \tag{8}$$

$$w^{NL}(z,s,n)=\bar{w}^{NL}-n\frac{\partial\bar{u}^{NL}}{\partial z};\qquad v^{NL}(z,s,n)=\bar{v}^{NL}-n\frac{\partial\bar{u}^{NL}}{\partial s};\qquad u^{NL}(z,s,n)=\bar{u}^{NL} \tag{9}$$

The only non-zero strain components, according to Bernoulli hypothesis, are:

$$e_{zz}=\frac{\partial w^L}{\partial z};\qquad e_{zs}=\frac{\partial w^L}{\partial s}+\frac{\partial v^L}{\partial z}; \tag{10}$$

$$\eta_{zz}=\frac{1}{2}\left[\left(\frac{\partial w^L}{\partial z}\right)^2+\left(\frac{\partial u^L}{\partial z}\right)^2+\left(\frac{\partial v^L}{\partial z}\right)^2\right];\qquad \eta_{zs}=\frac{\partial w^L}{\partial z}\frac{\partial w^L}{\partial s}+\frac{\partial u^L}{\partial z}\frac{\partial u^L}{\partial s}+\frac{\partial v^L}{\partial z}\frac{\partial v^L}{\partial s}; \tag{11}$$

$$\tilde{e}_{zz}=\frac{\partial w^{NL}}{\partial z};\qquad \tilde{e}_{zs}=\frac{\partial w^{NL}}{\partial s}+\frac{\partial v^{NL}}{\partial z} \tag{12}$$

where e_{ij} and η_{ij} are linear and non-linear strains with respect to linear displacements components, while $\tilde{e}_{ij}$ are linear strains with respect to nonlinear displacements.

By putting Eq. (8) into Eq. (10) follows:

$$e_{zz} = \frac{\partial w^L}{\partial z} = \frac{\partial \bar{w}^L}{\partial z} - n\frac{\partial^2 \bar{u}^L}{\partial z^2} = \bar{\varepsilon}_z{}^L + n \cdot \kappa_z{}^L \tag{13}$$

$$e_{zs} = \frac{\partial w^L}{\partial s} + \frac{\partial v^L}{\partial z} = \frac{\partial \bar{w}^L}{\partial s} + \frac{\partial \bar{v}^L}{\partial z} - 2n\frac{\partial^2 \bar{u}^L}{\partial s \partial z}\frac{\partial w^L}{\partial s} + \frac{\partial v^L}{\partial z} = \bar{\gamma}_{zs}^L - 2n\frac{\partial^2 \bar{u}^L}{\partial s \partial z} = \bar{\gamma}_{zs}^L + n \cdot \kappa_{zs}{}^L \quad . \tag{14}$$

The middle surface shear strain $\bar{\gamma}_{zs}^L$, in accordance with second assumption, will be:

$$\bar{\gamma}_{zs}^L = \frac{\partial \bar{w}^L}{\partial s} + \frac{\partial \bar{v}^L}{\partial z} = \frac{F_s}{t} \cdot \frac{d\varphi_z}{dz},$$

Where, t is the thickness of the box section contour and F_s is the St.Venant circuit flow. It should be noted that F_s is the section property independent of the choice of the coordinate system, pole and origin. The explicit forms of F_s for box section are given in Ref. [21].

The appropriate strains and curvatures can be expressed in the following form:

$$\bar{\varepsilon}_z{}^L = \frac{\partial \bar{w}^L}{\partial z} = w_o' - yv_o'' - xu_o'' - \omega\,\varphi_z'' \tag{15}$$

$$\kappa_z{}^L = -\frac{\partial^2 \bar{u}^L}{\partial z^2} = -u_o'' \sin\beta + v_o'' \cos\beta + \varphi_z'' \cdot q \tag{16}$$

$$\kappa_{zs}{}^L = 2\varphi_z' \tag{17}$$

so Eqs. (13) and (14) become:

$$e_{zz} = \varepsilon_z^0 + \kappa_y(x + n\sin\beta) + \kappa_x(y - n\cos\beta) + \kappa_\omega(\omega - nq) \tag{18}$$

$$e_{zs} = \left(n + \frac{F_s}{2t}\right)\kappa_{zs} \tag{19}$$

The axial strain and the biaxial curvatures in *x* and *y* direction, the warping curvature and the twisting curvature, are defined as:

$$\varepsilon_z^0 = w_o', \qquad \kappa_y = -u_o'', \qquad \kappa_x = -v_o'', \qquad \kappa_\omega = -\varphi_z'', \qquad \kappa_{sz} = 2\varphi_z'. \tag{20}$$

Analogously, the nonlinear strain components from Eqs. (11) and (12) can be expressed in terms of the relevant components of the beam displacement.

In Eqs. (16) and (18), *q* presents the distance of the contour radius from an arbitrary point P called pole, Fig. 1:

$$q = (x - x_P)\cos\beta + (y - y_P)\sin\beta \tag{21}$$

The warping function ω with respect to contour coordinate system, is given by [22, 23]:

$$\omega = \int_{s_0}^{s} \left[r - \frac{F_s}{t} \right] ds ; \quad \oint_i \frac{F_s}{t} ds = 2A_i , \qquad i = 1,...,n \tag{22}$$

Where r is height of triangle with the base ds ; A_i is the area circumscribed by the contour of *i*-th circuit.

The cross-section internal beam forces can be defined as:

$$F_z = \int_A \sigma_z \, dn\, ds , \quad M_x = \int_A \sigma_z (y - n\cos\beta) dnds , \quad M_y = \int_A \sigma_z (x + n\sin\beta) dnds$$

$$M_z = \int_A \tau_{zs} \left(n + \frac{F_s}{2t} \right) dnds , \quad M_\omega = \int_A \sigma_z (\omega - nq) dnds \tag{23}$$

where F_z represents the axial force, M_x and M_y are bending moments with respect to *x*- and *y*-axis, respectively, M_z is the torsion moment, while M_ω is the bimoment.

2.3. Constitutive equations

The material properties of FG box beams are assumed to vary continuously through the wall thickness by a power law according to [24]:

$$P(n) = (P_{out} - P_{in}) \cdot V_c + P_{in} \tag{24}$$

where *P* represents the effective material property such as Young's modulus *E* and Poisson's ratio *v*; subscripts *in* and *out* represent the inner and outer surface constituents, and V_c is the volume fraction of the ceramic phase, respectively. Three different types of FG box beams are considered as shown in Fig. 2:

1) Type A: the wall composed of FG material for which material varies from a metal-rich inner surface ($n = t_0 = -0.5t$) to a ceramic-rich outer surface ($n = t_3 = +0.5t$). The volume fraction of ceramic phase is defined as:

$$V_c = \left(\frac{1}{2} + \frac{n}{t} \right)^p , \qquad t_0 \le n \le t_3 \tag{25}$$

2) Type B: the sandwich wall with fully ceramic core and FG skins [25, 26]. The inner skin varies from a metal-rich surface ($n = t_0 = -0.5t$) to a ceramic-rich surface ($n = t_1$) while the outer skin varies from a ceramic-rich surface ($n = t_2$) to a metal-rich surface ($n = t_3 = +0.5t$). The volume fraction of ceramic phase is defined as:

$$V_c = \left(\frac{n - t_0}{t_1 - t_0}\right)^p, \qquad t_0 \le n \le t_1$$
$$V_c = 1, \qquad t_1 \le n \le t_2 \tag{26}$$
$$V_c = \left(\frac{n - t_3}{t_2 - t_3}\right)^p, \qquad t_2 \le n \le t_3$$

3) Type C: the sandwich wall with fully metal inner and fully ceramic outer skin, while the core is graded from metal to ceramic [27]. The volume fraction of ceramic phase is defined as:

$$V_c = \left(\frac{n - t_1}{t_2 - t_1}\right)^p, \qquad t_1 \le n \le t_2 \tag{27}$$

In expressions above Eqs. (25)-(27), p is the power-law index.

The stress-strain relation for elastic FGM box beam can be written as:

$$\sigma_z = E(n)\cdot\varepsilon_z, \qquad \tau_{zs} = \frac{E(n)}{2\left[1+\nu(n)\right]}\cdot\gamma_{zs} = G(n)\cdot\gamma_{zs} \tag{28}$$

Using Eqs. (18), (19) and (28), the beam components can be expressed in a matrix form as:

$$\begin{Bmatrix} F_z \\ M_y \\ M_x \\ M_\omega \\ M_T \end{Bmatrix} = \begin{bmatrix} R_{11} & R_{12} & R_{13} & R_{14} & 0 \\ R_{21} & R_{22} & R_{23} & R_{24} & 0 \\ R_{31} & R_{32} & R_{33} & R_{34} & 0 \\ R_{41} & R_{42} & R_{43} & R_{44} & 0 \\ 0 & 0 & 0 & 0 & R_{55} \end{bmatrix} \begin{Bmatrix} \varepsilon_z^0 \\ \kappa_y \\ \kappa_x \\ \kappa_\omega \\ \kappa_{sz} \end{Bmatrix} \tag{29}$$

where R_{ij} are FG box beam stiffnesses defined as:

$$R_{11} = \int_A E(n)\,dn\,ds, \tag{30a}$$

$$R_{12} = R_{21} = \int_A E(n)\,x\,dnds + \int_A E(n)\,n\sin\beta\,dnds, \tag{30b}$$

$$R_{13} = R_{31} = \int_A E(n)\,y\,dnds - \int_A E(n)\,n\cos\beta\,dnds, \tag{30c}$$

$$R_{14} = R_{41} = \int_A E(n)\,\omega\,dnds - \int_A E(n)\,n\,q\,dnds, \tag{30d}$$

$$R_{22} = \int_A E(n)\,x^2\,dnds - 2\int_A E(n)\,n\,x\sin\beta\,dnds + \int_A E(n)\,n^2\sin^2\beta\,dnds, \tag{30e}$$

$$R_{23} = R_{32} = \int_A E(n)\,xy\,dnds + \int_A E(n)\,n(y\sin\beta - x\cos\beta)\,dnds - \int_A E(n)\,n^2\sin\beta\cos\beta\,dnds, \tag{30f}$$

$$R_{24} = R_{42} = \int_A E(n)\,x\omega\,dnds + \int_A E(n)\,n(\omega\sin\beta - xq)\,dnds - \int_A E(n)\,n^2\,q\sin\beta\,dnds, \tag{30g}$$

$$R_{33} = \int_A E(n)\, y^2\, dnds - 2\int_A E(n)\, n\, y \cos\beta\, dnds + \int_A E(n)\, n^2 \cos^2\beta\, dnds\,, \tag{30h}$$

$$R_{34} = R_{43} = \int_A E(n)\, y\omega\, dnds - \int_A E(n)\, n(\omega\cos\beta + yq)\, dnds + \int_A E(n)\, n^2\, q\cos\beta\, dnds\,, \tag{30i}$$

$$R_{44} = \int_A E(n)\, \omega^2\, dnds - 2\int_A E(n)\, n\, q\omega\, dnds + \int_A E(n)\, n^2 q^2 dnds\,, \tag{30j}$$

$$R_{55} = \int_A \frac{F_s^{\,2}}{4t^2} G(n)\; dnds + \int_A \frac{F_s}{t} G(n)\, n\; dnds + \int_A G(n)\, n^2 dnds\;\; . \tag{30k}$$

3. Finite element formulation

Fig. 3 shows the 14 degree of freedom beam finite element with two nodes A and B. The appropriate displacement and force components are defined for centroid O. The nodal displacement and nodal force vectors are:

$$\left(\mathbf{u}^{\mathrm{e}}\right)^{\mathrm{T}} = \left\{ w_{\mathrm{A}}\; u_{\mathrm{A}}\; v_{\mathrm{A}}\; \varphi_{\mathrm{zA}}\; \varphi_{\mathrm{xA}}\; \varphi_{\mathrm{yA}}\; w_{\mathrm{B}}\; u_{\mathrm{B}}\; v_{\mathrm{B}}\; \varphi_{\mathrm{zB}}\; \varphi_{\mathrm{xB}}\; \varphi_{\mathrm{yB}}\; \theta_{\mathrm{A}}\; \theta_{\mathrm{B}} \right\}, \tag{31}$$

$$\left(\mathbf{f}^{\mathrm{e}}\right)^{\mathrm{T}} = \left\{ F_{\mathrm{zA}}\; F_{\mathrm{xA}}\; F_{\mathrm{yA}}\; M_{\mathrm{zA}}\; M_{\mathrm{xA}}\; M_{\mathrm{yA}}\; F_{\mathrm{zB}}\; F_{\mathrm{xB}}\; F_{\mathrm{yB}}\; M_{\mathrm{zB}}\; M_{\mathrm{xB}}\; M_{\mathrm{yB}}\; M_{\omega\mathrm{A}}\; M_{\omega\mathrm{B}} \right\}. \tag{32}$$

Where the superscript ”e“ denotes the e-th finite element.

According to the incremental description, it is necessary to subdivide a load–deformation path of a finite element into a number of steps or increments where three equilibrium configurations can be recognized: the initial configuration C_0, the last calculated equilibrium configuration C_1 and current unknown configuration C_2. By the UL formulation adopted in this paper, each system quantity occurring in C_2 can be expressed with reference to C_1. Hereafter, a left superscript denotes the configuration in which a quantity occurs, and a left subscript the configuration in which the quantity is measured. If the superscript and subscript of a quantity are same, the latter may be dropped. The absence of the superscript indicates that the quantity is an increment between C_1 and C_2 [28].

Applying the virtual work principle, the linearized incremental equilibrium equations of an elastic beam element can be written as:

$$\delta \mathsf{U}_{\mathrm{E}} + \delta \mathsf{U}_{\mathrm{G}} = \delta\, {}^{2}\mathsf{W} - \delta\, {}^{1}\mathsf{W} \tag{33}$$

where the left-hand side represents the internal work composed of the virtual incremental elastic strain energy:

$$\delta \mathsf{U}_{\mathrm{E}} = \int_{{}^{1}V} {}_{1}C_{ijkl}\; {}_{1}e_{kl}\; \delta\, {}_{1}e_{ij}\; {}^{1}\mathrm{d}V \tag{34}$$

and the virtual geometric incremental potential:

$$\delta \mathsf{U}_{\mathrm{G}} = \int\limits_{{}^1V} {}^1S_{ij}\, \delta_1 \eta_{ij}\ {}^1\mathrm{d}V + \int\limits_{V} {}^1S_{ij}\, \delta_1 \tilde{e}_{ij}\ {}^1\mathrm{d}V - \int\limits_{{}^1A_\sigma} {}^1t_i\, \delta \tilde{u}_i\ {}^1\mathrm{d}A_\sigma \tag{35}$$

while the terms on the right-hand side represent the virtual work done by the external forces at the end and beginning of the current increment, respectively,

$$\delta\, {}^2\mathsf{W} = \int\limits_{{}^1A_\sigma} {}^2t_i\, \delta u_i\ {}^1\mathrm{d}A_\sigma\ , \quad \delta\, {}^1\mathsf{W} = \int\limits_{{}^1V} {}^1S_{ij}\, \delta_1 e_{ij}\ {}^1\mathrm{d}V = \int\limits_{{}^1A_\sigma} {}^1t_i\, \delta u_i\ {}^1\mathrm{d}A_\sigma \tag{36}$$

In the preceding equations S_{ij} and t_{i} are, respectively, the second Piola-Kirchhoff stress tensor and surface tractions, C_{ijkl} is the constitutive or stress-strain tensor, while the symbol ‘‘δ’’ denotes the virtual quantities. Adopting a linear interpolation for w_{o} displacement and cubic interpolation for $u_0, v_0, \varphi_{\mathrm{z}}$ one can derive:

$$\delta \mathsf{U}_{\mathrm{E}} = \int\limits_{V} S_{\mathrm{ij}}\, \delta e_{\mathrm{ij}}\, \mathrm{d}V = \left(\delta \mathbf{u}^{\mathrm{e}}\right)^{\mathrm{T}} \mathbf{k}_{\mathrm{E}}^{\mathrm{e}}\ \mathbf{u}^{\mathrm{e}}, \tag{37}$$

$$\delta \mathsf{U}_{\mathrm{G}} = \int\limits_{V} S_{\mathrm{ij}} \left(\delta \eta_{\mathrm{ij}} + \delta \tilde{e}_{\mathrm{ij}}\right) \mathrm{d}V - \int\limits_{A_\sigma} t_{\mathrm{i}}\, \delta \tilde{u}_{\mathrm{i}}\, \mathrm{d}A_\sigma = \left(\delta \mathbf{u}^{\mathrm{e}}\right)^{\mathrm{T}} \mathbf{k}_{\mathrm{G}}^{\mathrm{e}}\ \mathbf{u}^{\mathrm{e}}, \tag{38}$$

$$\delta \mathsf{W} = \int\limits_{V} S_{\mathrm{ij}}\, \delta e_{\mathrm{ij}}\, \mathrm{d}V = \left(\delta \mathbf{u}^{\mathrm{e}}\right)^{\mathrm{T}} \mathbf{f}^{\mathrm{e}}. \tag{39}$$

where $\mathbf{k}_{\mathrm{E}}^{\mathrm{e}}$ and $\mathbf{k}_{\mathrm{G}}^{\mathrm{e}}$ are (14×14) elastic and geometric stiffness matrices of beam element while $\mathbf{f}^{\mathrm{e}}$ is a nodal force vector respectively. The explicit forms of the terms arising from nonlinear components are given in Ref. [29]. The set of non-linear equilibrium equations of a structure must be attempted by incremental iterative approach. This procedure is described in Ref. [28].

4. Results

4.1 Thin-walled FG sandwich box beam

A thin-walled FG sandwich box beam with length L = 8 m, width b = 0.2 m, height h = 0.1 m and wall thickness t = 0.005 m is considered to investigate the effects of power-law index, skin-core-skin thickness ratios and boundary conditions on the critical buckling loads and post-buckling responses. FG material properties are assumed to be [16]: Aluminum (Al: $E_{\mathrm{m}} = E_{\mathrm{in}}$ = 70 GPa, ν_{m} = 0.3) and Alumina (Al_2O_3: $E_{\mathrm{c}} = E_{\mathrm{out}}$ = 380 GPa, ν_{c} = 0.3). The beam is modeled using the eight beam finite elements.

As the first example, the critical buckling loads of FG box beams (Type A) with different value of power law index p for three types of boundary conditions, clamped-clamped (C-C), clamped-free (C-F) and

simply-supported (S-S) are given in Table 1. Since all the coupling stiffnesses vanish in this case, the present results are in good agreement with the solutions in theoretical formula: $F_z = \pi^2 R_{ii} \big/ \left(kL\right)^2, \quad i = 2,3$ with k is effective-length factor, depends on boundary conditions; thus accuracy of the present model is established. As expected, an increase of the power-law index results in a decrease of elasticity modulus and bending rigidity, which leads to reduction in critical buckling loads. This reduction is recognizable for all three considered boundaries. It should be noted that for zero value of power-law index, the FG material is the full ceramic, while as the power-law index increases, the FG material tends towards the full metal.

In the next example, FG sandwich box beams of Types B and C are analysed. Three different skin-core-skin ratios (1-1-1, 1-2-1 and 2-2-1) for both types are considered. The obtained critical buckling loads are given in Tables 2 and 3. It can be observed that as power-law index increases, the critical buckling loads decreases in all cases. However the rate of decrease is directly dependent on skin-core-skin ratios in box beam wall. The material distribution has a significant effect on critical buckling load of box beam for all boundary conditions and for both buckling modes. It can be observed from Figs. 4-6 representing the critical buckling loads vs power-law index. In six cases considered, the smallest and largest critical buckling loads for both Types B and C correspond to (1-2-1) and (2-2-1), since they has the highest and lowest portion of ceramic phase comparing with others.

In order to demonstrate the stability and robustness of the algorithm, the responses of FG box beams are additionally monitored in nonlinear manner. To initiate buckling, a lateral perturbation force $\Delta F = 0.001\ F$ is applied at free end in C-F case and at the mid-span point in the S-S and C-C cases. The curves obtained in nonlinear manner representing the displacements of perturbation force point *vs* axial force are presented in Figs. 7-9 for Type A with power-law index $p = 0.5$ and $p = 5$, while in Figs. 10-12 for Types B and C with $p = 5$. As can be seen, the load-deflection curves correspond well to previously obtained critical buckling loads in terms of the rapid increase of lateral displacements when approaching the level of forces that correspond to the critical values calculated in eigenvalue manner.

4.2 Thin-walled FG sandwich box frame

The L-shaped frame of the same material types and box section 200 mm × 100 mm × 5 mm is considered, Fig. 13. The frame is cantilevered at point A and loaded by a single concentrated load at free end C in X direction. The warping at junction point B is supposed to be fully restrained. Obtained critical buckling

loads are given in Table 4. For validation purposes, the critical loads for full ceramic $F\mathrm{cr}_{(Al_2O_3)} = 385305$ N and full metal $F\mathrm{cr}_{(Al)} = 70977$ N sections are calculated by MASTAN2 structural analysis program [30]. Since for power-law index $p = 0$ the A and B-types correspond to full ceramic as well as for $p = 1000$ the A-type tends to full metal, the good agreement of results are evident. Fig. 14 represents the critical buckling loads versus power-law index for all 7 cross section types. The lowest critical buckling modes correspond to lateral, Fig. 15., for all cases. In order to perform post-buckling responses, a small perturbation force of 0.001 *F* acting in Z-axis direction at point C is simultaneously introduced to initiate lateral buckling. The results obtained for Type A for various values of power-law index are shown in Fig. 16. As can be seen, both limit cases, full metal $p = 1000$ as well as full ceramic $p = 0$ correspond well to linearised buckling loads. Load versus lateral displacement of point C for power-law index value $p = 5$ for all Types A, B and C are also plotted on Fig. 17.

5. Conclusion

The paper has presented an effective numerical beam model capable to analyze the global buckling behaviour of thin-walled functionally graded box beams whose material properties are assumed to vary in the thickness direction according to power law. Three different types of box beam wall are considered: FG wall, sandwich wall with FG skin-homogeneous core and sandwich wall with homogeneous skin-FG core. Effects of power law index, skin-core-skin thickness ratios and boundary conditions on the critical buckling loads and post-buckling responses are observed. Since the previous works in this area [16] are engaged in simulations of free vibration analysis, this paper as novel aspect simulate the buckling behaviour of subject beams. The present model is appropriate and efficient in analyzing buckling problem of FGM box beam type structures.

Acknowledgement

The first and the third author gratefully acknowledge financial support from Croatian Science Foundation under project “6876 Assessment of structural behaviour in limit state operating conditions“ (O-1673-2014). The second and fourth author gratefully acknowledges financial support by the Basic Research Laboratory

Program of the National Research Foundation of Korea (NRF) funded by the Ministry of Education, Science and Technology (2010-0019373 and 2012R1A2A1A01007450).

References

[1] B. V. Sankar, An elasticity solution for functionally graded beams, Composites Science and Technology 61 (5) (2001) 689 – 696.

[2] A. Chakraborty, S. Gopalakrishnan, J. N. Reddy, A new beam finite element for the analysis of functionally graded materials, International Journal of Mechanical Sciences 45 (3) (2003) 519 –539.

[3] M. Aydogdu, V. Taskin, Free vibration analysis of functionally graded beams with simply supported edges, Materials & Design 28 (5) (2007) 1651 – 1656.

[4] S. Kapuria, M. Bhattacharyya, A. N. Kumar, Bending and free vibration response of layered functionally graded beams: A theoretical model and its experimental validation, Composite Structures 82 (3) (2008) 390 – 402.

[5] X.-F. Li, A unified approach for analyzing static and dynamic behaviors of functionally graded Timoshenko and Euler-Bernoulli beams, Journal of Sound and Vibration 318 (4-5) (2008) 1210–1229.

[6] S. A. Sina, H. M. Navazi, H. Haddadpour, An analytical method for free vibration analysis of functionally graded beams, Materials & Design 30 (3) (2009) 741 – 747.

[7] M. Simsek, Fundamental frequency analysis of functionally graded beams by using different higher-order beam theories, Nuclear Engineering and Design 240 (4) (2010) 697 – 705.

[8] A. E. Alshorbagy, M. Eltaher, F. Mahmoud, Free vibration characteristics of a functionally graded beam by finite element method, Applied Mathematical Modelling 35 (1) (2011) 412 – 425.

[9] H.-T. Thai, T. P. Vo, Bending and free vibration of functionally graded beams using various higher-order shear deformation beam theories, International Journal of Mechanical Sciences 62 (1) (2012) 57–66.

[10] T. P. Vo, H.-T. Thai, T.-K. Nguyen, F. Inam, Static and vibration analysis of functionally graded beams using refined shear deformation theory, Meccanica (2013) 1–14.

[11] M. C. Amirani, S. M. R. Khalili, N. Nemati, Free vibration analysis of sandwich beam with FG core using the element free Galerkin method, Composite Structures 90 (3) (2009) 373 – 379.

[12] T. Q. Bui, A. Khosravifard, C. Zhang, M. R. Hematiyan, M. V. Golub, Dynamic analysis of sandwich beams with functionally graded core using a truly meshfree radial point interpolation method, Engineering Structures 47 (2013) 90 – 104.

[13] T. P. Vo, H.-T. Thai, T.-K. Nguyen, A. Maheri, J. Lee, Finite element model for vibration and buckling of functionally graded sandwich beams based on a refined shear deformation theory, Engineering Structures 64 (2014) 12 – 22.

[14] L. Librescu, S.-Y. Oh, O. Song, Thin-walled beams made of functionally graded materials and operating in a high temperature environment: Vibration and stability, Journal of Thermal Stresses 28 (6-7) (2005) 649–712.

[15] M. T. Piovan, S. P. Machado, Thermoelastic dynamic stability of thin-walled beams with graded material properties, Thin-Walled Structures 49 (3) (2011) 437 – 447.

[16] N. Ziane, S. A. Meftah, H. A. Belhadj, A. Tounsi, E. A. A. Bedia, Free vibration analysis of thin and thick-walled FGM box beams, International Journal of Mechanical Sciences 66 (2013) 273 – 282.

[17] E. C. Carvalho, P. B. Goncalves, G. Rega, Z. J. G. N. Del Prado, Nonlinear nonplanar vibration of a functionally graded box beam, Meccanica (2014) 1–25.

[18] D. S. Mashat, E. Carrera, A. M. Zenkour, S. A. A. Khateeb, M. Filippi, Free vibration of FGM layered beams by various theories and finite elements, Composites Part B: Engineering 59 (2014) 269 – 278.

[19] D. Lanc, G. Turkalj, I. Pesic, Global buckling analysis model for thin-walled composite laminated beam type structures, Composite Structures 111 (2014) 371 – 380.

[20] WF Chen, T Atsuta. Theory of beam–columns. Vol. 2: Space behavior and design, J. Ross Publishing, Fort Lauderdale (2008)

[21] Vo TP, Lee J. Flexural-torsional behavior of thin-walled closed-section composite box beams. Eng. Struct, 2007; 29: 1774–1782.

[22] Gjelsvik A. The theory of thin-walled bars. New York: Wiley; 1981.

[23] Vo TP, Lee J, Ahn N. On sixfold coupled vibrations of thin-walled composite box beams. Composite structures, 2009; 89(4): 524-535.

[24] Reddy JN. Mechanics of laminated composite plates and shells: theory and analysis. CRC Press, Boca Raton, 2004.

[25] Zenkour, A. M. A comprehensive analysis of functionally graded sandwich plates: Part 2-Buckling

and free vibration International Journal of Solids and Structures, 2005, 42, 5243 - 5258

[26] Zenkour, A. M. A comprehensive analysis of functionally graded sandwich plates: Part 1-Deflection and stresses International Journal of Solids and Structures, 2005, 42, 5224 - 5242

[27] Neves, A. M. A.; Ferreira, A. J. M.; Carrera, E.; Cinefra, M.; Roque, C. M. C.; Jorge, R. M. N. & Soares, C. M. M. Static, free vibration and buckling analysis of isotropic and sandwich functionally graded plates using a quasi-3D higher-order shear deformation theory and a meshless technique Composites Part B: Engineering , 2013, 44, 657 - 674

[28] Turkalj G, Brnic J, Kravanja S. A beam model for large displacement analysis of flexibly connected thin-walled beam-type structures. Thin-Walled structures, 2011; 49:1007-1016.

[29] Turkalj G, Brnic J, Prpic-Orsic J. Large rotation analysis of elastic thin-walled beam-type structures using ESA approach. Computers & Structures, 2003; 81(18-19): 1851-1864.

[30] McGuire W, Gallagher RH, Ziemian R. Matrix structural analysis, With MASTAN2, New York: JohnWiley & Sons, 2000.

CAPTIONS OF TABLES

Table 1: Buckling loads (MN) of FG box beam (Type A) with various values of power-law index for different boundary conditions.
Table 2: Buckling loads (MN)of FG sandwich box beam of Type B with various values of power-law index for different boundary conditions.
Table 3: Buckling loads (MN) of FG sandwich box beam of Type C with various values of power-law index for different boundary conditions.
Table 4: Buckling loads (MN) of *L*-frame (Types A, B and C) for various values of power-law index.

Table 1: Buckling loads (MN) of FG box beam (Type A) with various values of power-law index for different boundary conditions.

BC	Mode	Method	Power-law index p							
			0	0.2	0.5	1	2	5	10	1000
C-F	Y	Present	0.08552	0.07435	0.06306	0.05163	0.04001	0.02810	0.02255	0.01583
		Formula	0.08561	0.07435	0.06306	0.05163	0.04001	0.02810	0.02255	0.01583
	X	Present	0.24420	0.21146	0.17859	0.14559	0.11239	0.07890	0.06355	0.04519
		Formula	0.24438	0.21146	0.17859	0.14559	0.11239	0.07890	0.06355	0.04519
S-S	Y	Present	0.34209	0.29740	0.25225	0.20654	0.16004	0.11240	0.09022	0.06332
		Formula	0.34245	0.29737	0.25224	0.20653	0.16003	0.11242	0.09022	0.06332
	X	Present	0.97683	0.84587	0.71439	0.58237	0.44956	0.31562	0.25421	0.18076
		Formula	0.97753	0.84585	0.71436	0.58235	0.44955	0.31613	0.25420	0.18076
C-C	Y	Present	1.36903	1.19017	1.00947	0.82655	0.64047	0.44982	0.36105	0.25340
		Formula	1.36979	1.18956	1.00896	0.82613	0.64014	0.44958	0.36087	0.25327
	X	Present	3.90921	3.38512	2.85891	2.33061	1.79912	1.26307	1.01732	0.72340
		Formula	3.91014	3.38338	2.85744	2.32941	1.79820	1.26242	1.01680	0.72303

Table 2: Buckling loads (MN) of FG sandwich box beam of Type B with various values of power-law index for different boundary conditions.

Type B	BC	Mode	Power-law index p							
			0	0.2	0.5	1	2	5	10	1000
1-1-1	C-F	Y	0.08552	0.07776	0.07001	0.06225	0.05450	0.04674	0.04322	0.03899
		X	0.24420	0.22206	0.19993	0.17779	0.15565	0.13352	0.12346	0.11138
	S-S	Y	0.34209	0.31106	0.28003	0.24901	0.21799	0.18698	0.17289	0.15598
		X	0.97683	0.88828	0.79973	0.71117	0.62263	0.53408	0.49384	0.44554
	C-C	Y	1.36903	1.24484	1.12067	0.99651	0.87238	0.74829	0.69189	0.62423
		X	3.90921	3.55482	3.20043	2.84606	2.49170	2.13735	1.97629	1.78303
1-2-1	C-F	Y	0.08552	0.07970	0.07388	0.06807	0.06225	0.05643	0.05379	0.05062
		X	0.24420	0.22760	0.21099	0.19439	0.17779	0.16119	0.15364	0.14458
	S-S	Y	0.34209	0.31882	0.29554	0.27227	0.24900	0.22574	0.21517	0.20248
		X	0.97683	0.91042	0.84400	0.77758	0.71117	0.64476	0.61457	0.57835
	C-C	Y	1.36903	1.27587	1.18273	1.08959	0.99648	0.90338	0.86107	0.81031
		X	3.90921	3.64341	3.37761	3.11182	2.84604	2.58027	2.45947	2.31451
2-2-1	C-F	Y	0.08552	0.07867	0.07181	0.06494	0.05804	0.05110	0.04794	0.04412
		X	0.24420	0.22441	0.20461	0.18479	0.16495	0.14507	0.13602	0.12514
	S-S	Y	0.34209	0.31470	0.28726	0.25975	0.23215	0.20443	0.19176	0.17650
		X	0.97683	0.89767	0.81846	0.73917	0.65980	0.58029	0.54409	0.50058
	C-C	Y	1.36903	1.25940	1.14958	1.03950	0.92906	0.81810	0.76742	0.70635
		X	3.90921	3.59240	3.27539	2.95811	2.64046	2.32228	2.17741	2.00329

Table 3: Buckling loads (MN) of FG sandwich box beam of Type C with various values of power-law index for different boundary conditions.

Type C	BC	Mode	Power-law index p							
			0	0.2	0.5	1	2	5	10	1000
1-1-1	C-F	Y	0.06359	0.05976	0.05593	0.05208	0.04820	0.04430	0.04251	0.04037
		X	0.17912	0.16810	0.15708	0.14603	0.13497	0.12387	0.11881	0.11279
	S-S	Y	0.25435	0.23906	0.22372	0.20831	0.19282	0.17720	0.17004	0.16148
		X	0.71650	0.67244	0.62832	0.58414	0.53988	0.49548	0.47525	0.45117
	C-C	Y	1.01789	0.95669	0.89529	0.83364	0.77163	0.70912	0.68048	0.64623
		X	2.86738	2.69103	2.51449	2.33769	2.16054	1.98288	1.90190	1.80554
1-2-1	C-F	Y	0.06919	0.06349	0.05777	0.05201	0.04620	0.04031	0.03761	0.03436
		X	0.19551	0.17903	0.16251	0.14596	0.12936	0.11269	0.10508	0.09601
	S-S	Y	0.27677	0.25398	0.23108	0.20803	0.18479	0.16126	0.15044	0.13745
		X	0.78207	0.71613	0.65007	0.58387	0.51747	0.45078	0.42034	0.38407
	C-C	Y	1.10761	1.01639	0.92475	0.83253	0.73952	0.64536	0.60205	0.55007
		X	3.12980	2.86587	2.60152	2.33658	2.07086	1.80399	1.68216	1.53702
2-2-1	C-F	Y	0.05904	0.05439	0.04972	0.04502	0.04029	0.03552	0.03333	0.03070
		X	0.16595	0.15266	0.13936	0.12603	0.11267	0.09926	0.09315	0.08587
	S-S	Y	0.23618	0.21756	0.19887	0.18008	0.16117	0.14207	0.13331	0.12281
		X	0.66381	0.61066	0.55744	0.50413	0.45069	0.39706	0.37261	0.34349
	C-C	Y	1.93657	1.78388	1.63062	1.47659	1.32151	1.16492	1.09305	1.00701
		X	2.65649	2.44379	2.23082	2.01747	1.80361	1.58901	1.49114	1.37461

Table 4: Buckling loads (MN) of *L*-frame (Types A, B and C) for various values of power-law index.

Type	Power-law index *p*							
	0	0.2	0.5	1	2	5	10	1000
A	0.386528	0.335173	0.283525	0.231504	0.178960	0.125661	0.101086	0.072059
B 1-1-1	0.386528	0.351471	0.316418	0.281368	0.246325	0.211288	0.195365	0.176260
B 1-2-1	0.386528	0.360233	0.333939	0.307648	0.281361	0.255078	0.243133	0.228801
B 2-2-1	0.386528	0.355332	0.324105	0.292835	0.261506	0.230093	0.215775	0.198551
C 1-1-1	0.284912	0.267535	0.250125	0.232674	0.215164	0.197570	0.189535	0.179957
C 1-2-1	0.310634	0.284666	0.258626	0.232491	0.206225	0.179771	0.167660	0.153192
C 2-2-1	0.264179	0.243148	0.222071	0.200931	0.179707	0.158361	0.148603	0.136961

CAPTIONS OF FIGURES

Figure 1: Contour displacements with respect to beam displacements.
Figure 2: Cross-section of thin-walled FG sandwich box beams (Types A, B and C).
Figure 3: Beam element: nodal displacements and nodal forces.
Figure 4: Critical buckling loads vs. power-law index for clamped-free boundary conditions (Types A, B and C).
Figure 5: Critical buckling loads vs. power-law index for simply-supported boundary conditions (Types A, B and C).
Figure 6: Critical buckling loads vs. power-law index for clamped-clamped boundary conditions.
Figure 7: Load vs. displacement with the power-law index values p = 0.5 and p = 5 for clamped-free boundary conditions (Type A).
Figure 8: Load vs. displacement with the power-law index values p = 0.5 and p = 5 for simply supported boundary conditions (Type A).
Figure 9: Load vs. displacement with the power-law index values p = 0.5 and p = 5 for clamped-clamped boundary conditions (Type A).
Figure 10: Load vs. displacement with the power-law index value p = 5 for clamped-free boundary conditions (Types B and C).
Figure 11: Load vs. displacement with the power-law index value p = 5 for simply supported boundary conditions (Types B and C).
Figure 12: Load vs. displacement with the power-law index value p = 5 for clamped-clamped boundary conditions (Types B and C).
Figure 13: L-frame.
Figure 14: Critical buckling loads vs. power-law index for L-frame (Types A, B and C).
Figure 15: L-frame lateral buckling mode.
Figure 16: Load vs. displacement for L-frame (Type A) for various values of power-law index.
Figure 17: Load vs. displacement with the power-law index value p = 5 for L-frame (Types A, B and C).

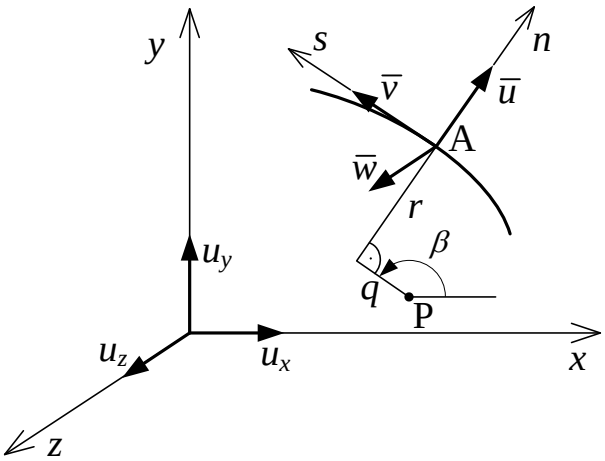

Figure 1: Contour displacements with respect to beam displacements

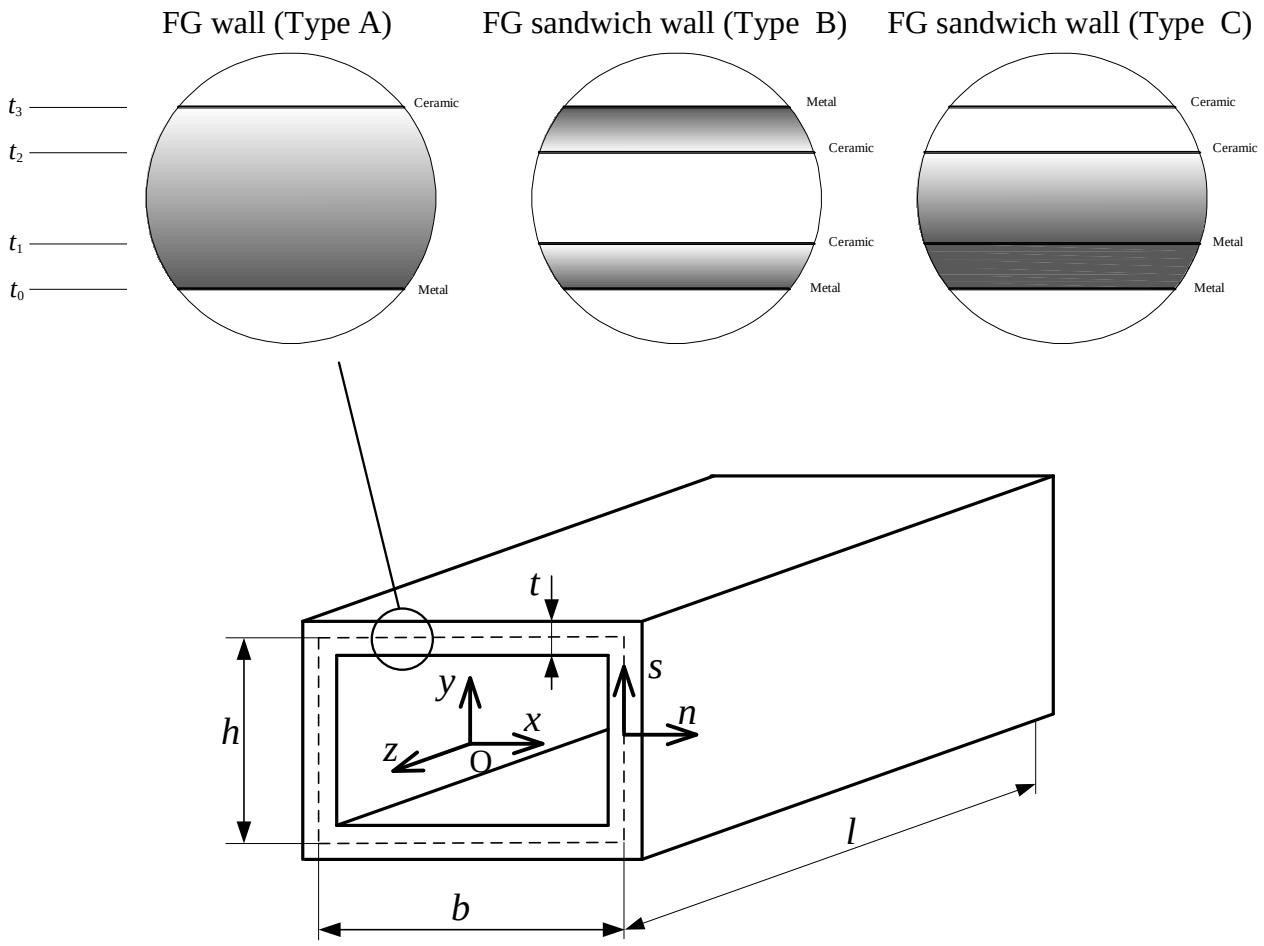

Figure 2: Cross-section of thin-walled FG sandwich box beams (Types A, B and C).

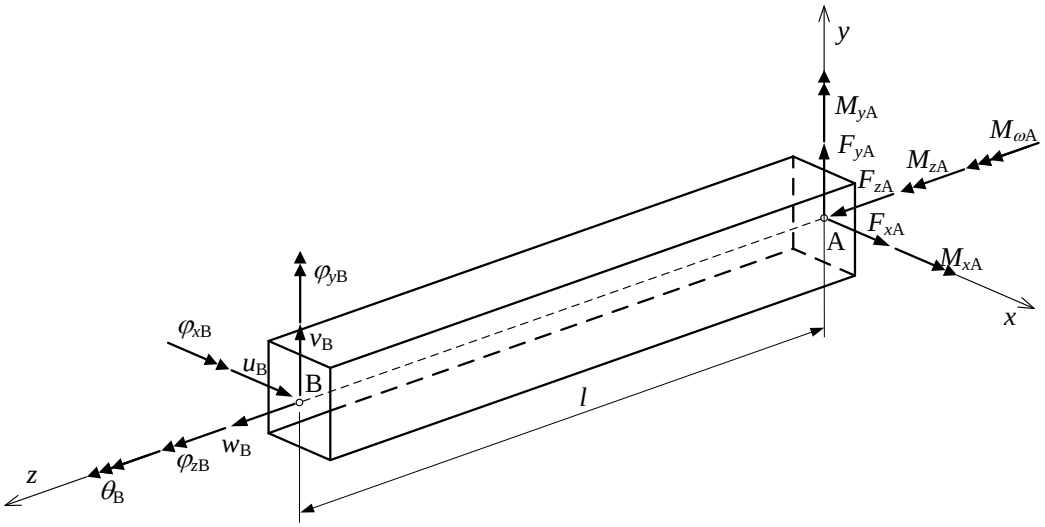

Figure 3: Beam element: nodal displacements and nodal forces.

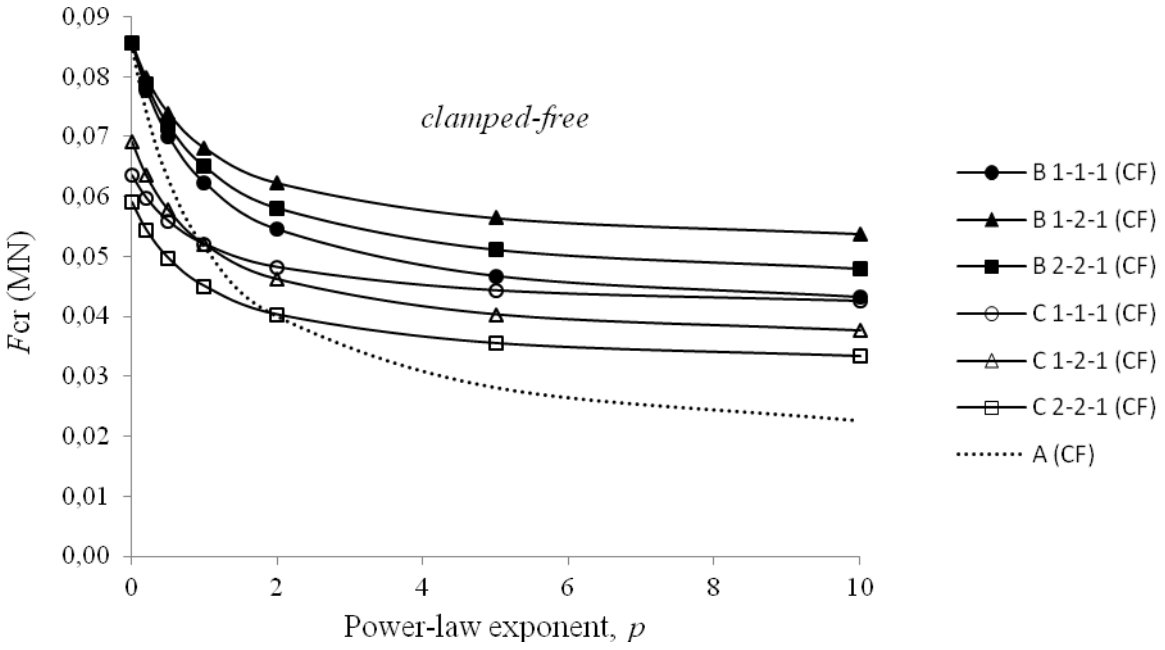

Figure 4: Critical buckling loads vs. power-law index for clamped-free boundary conditions (Types A, B and C).

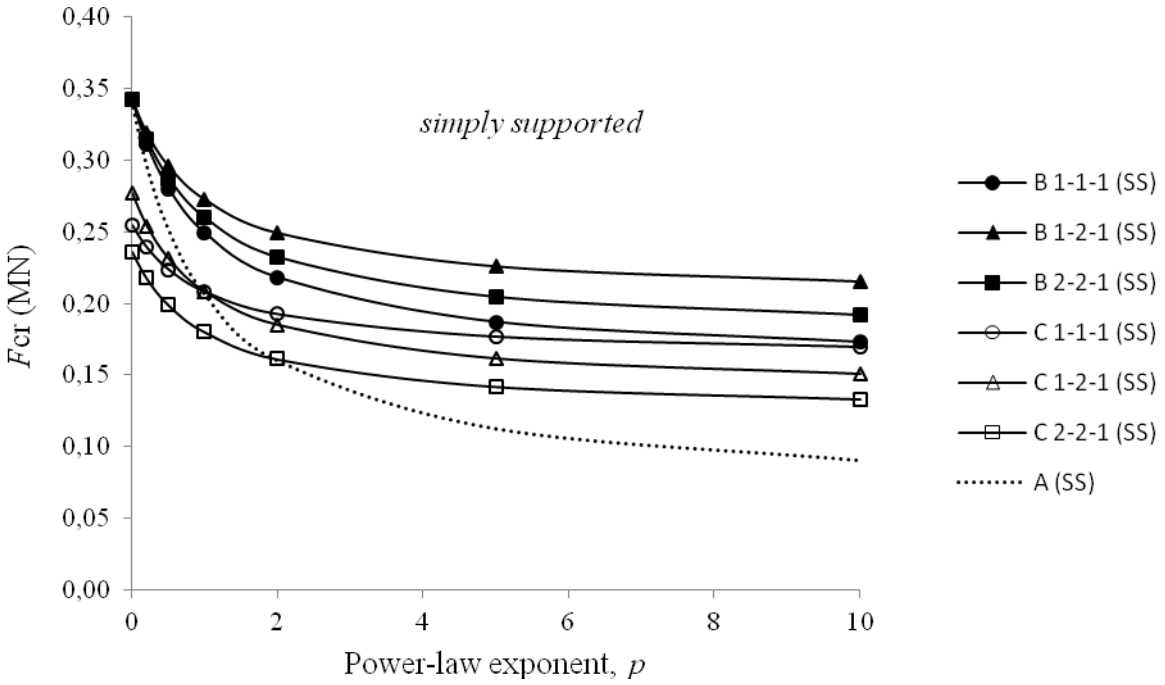

Figure 5: Critical buckling loads vs. power-law index for simply-supported boundary conditions (Types A, B and C).

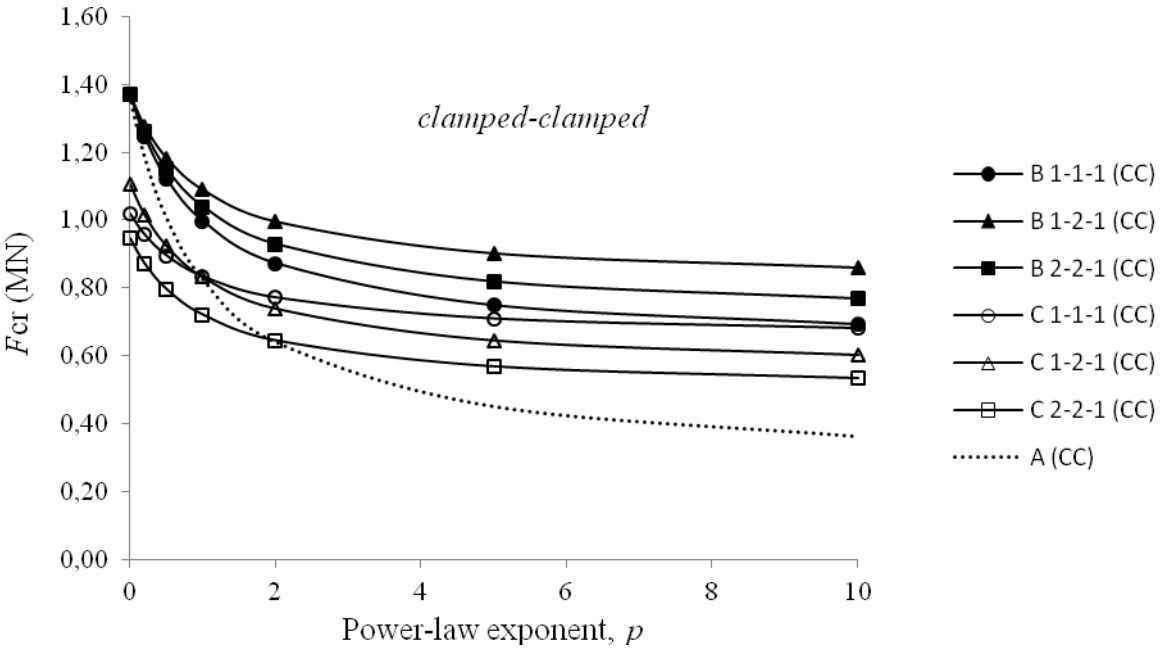

Figure 6: Critical buckling loads vs. power-law index for clamped-clamped boundary conditions (Types A, B and C).

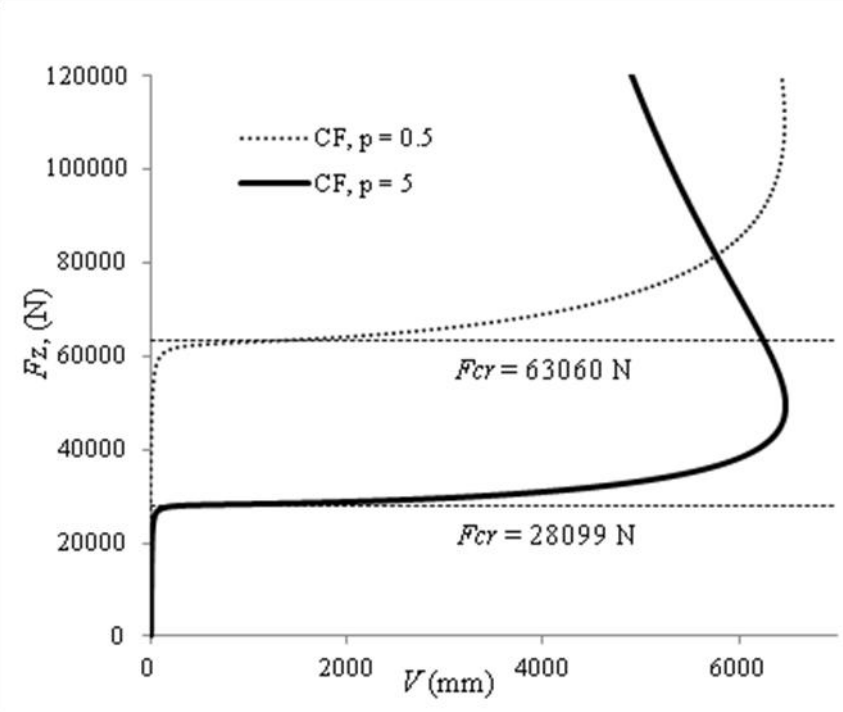

Figure 7: Load vs. displacement with the power-law index values $p = 0.5$ and $p = 5$ for clamped-free boundary conditions (Type A).

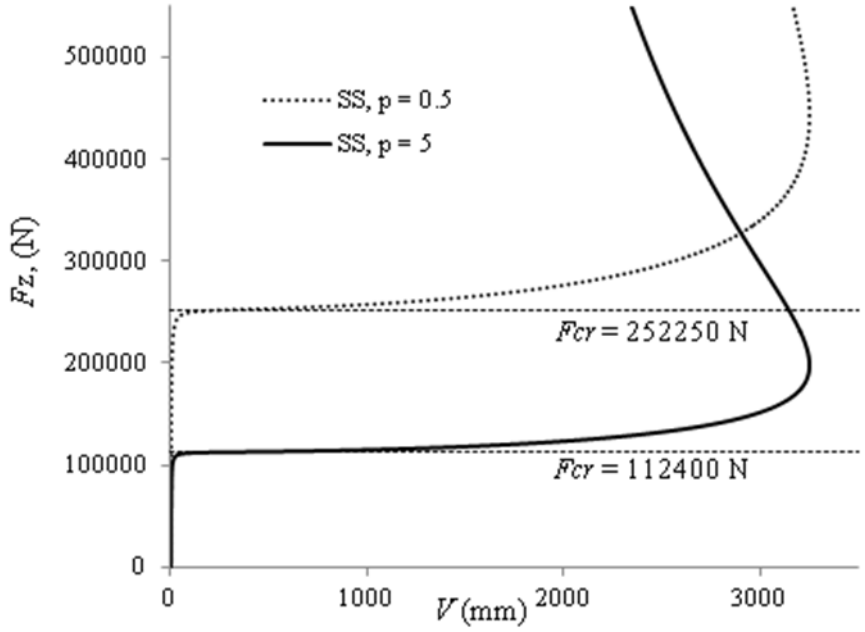

Figure 8: Load vs. displacement with the power-law index values p = 0.5 and p = 5 for simply supported boundary conditions (Type A).

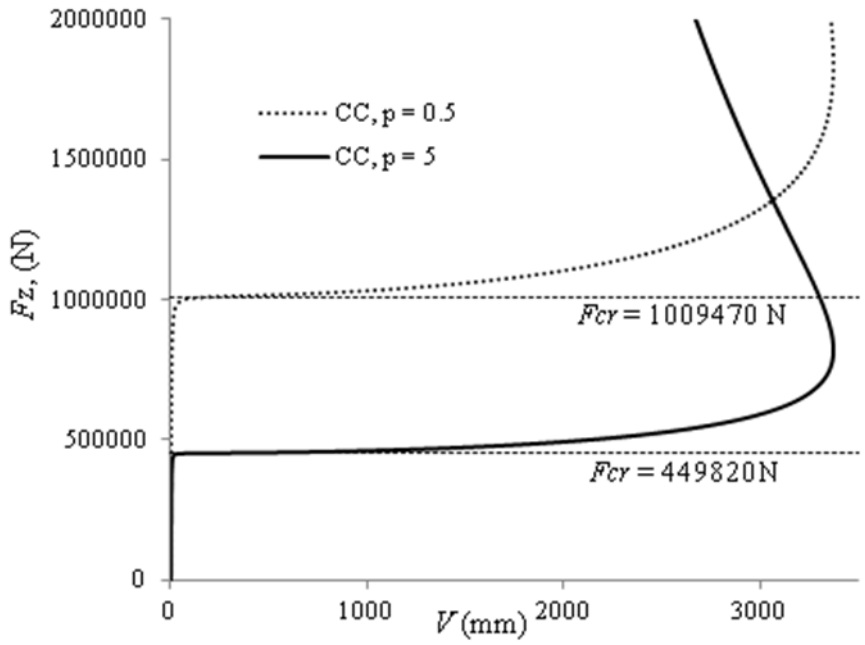

Figure 9: Load vs. displacement with the power-law index values $p = 0.5$ and $p = 5$ for clamped-clamped boundary conditions (Type A).

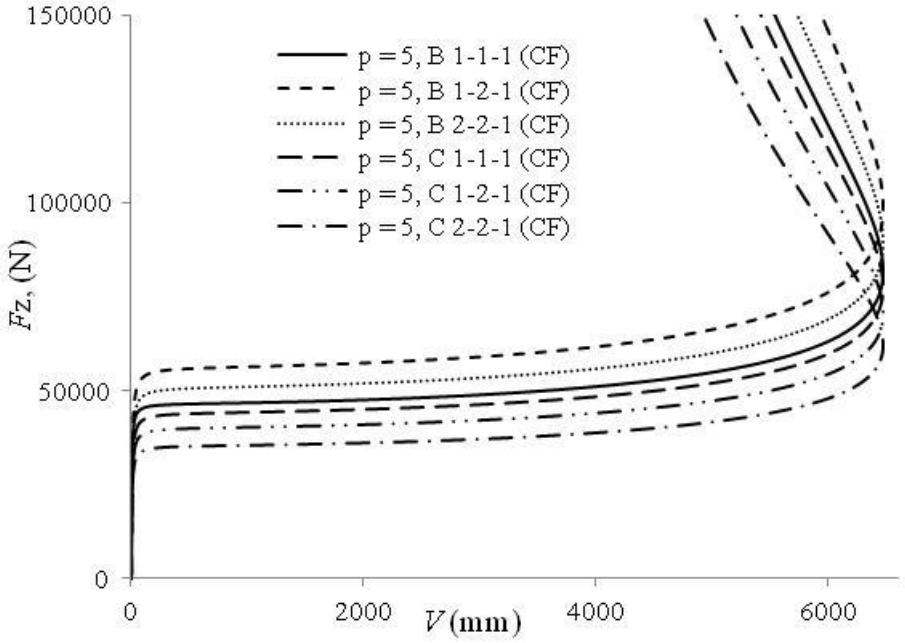

Figure 10: Load vs. displacement with the power-law index value p = 5 for clamped-free boundary conditions (Types B and C).

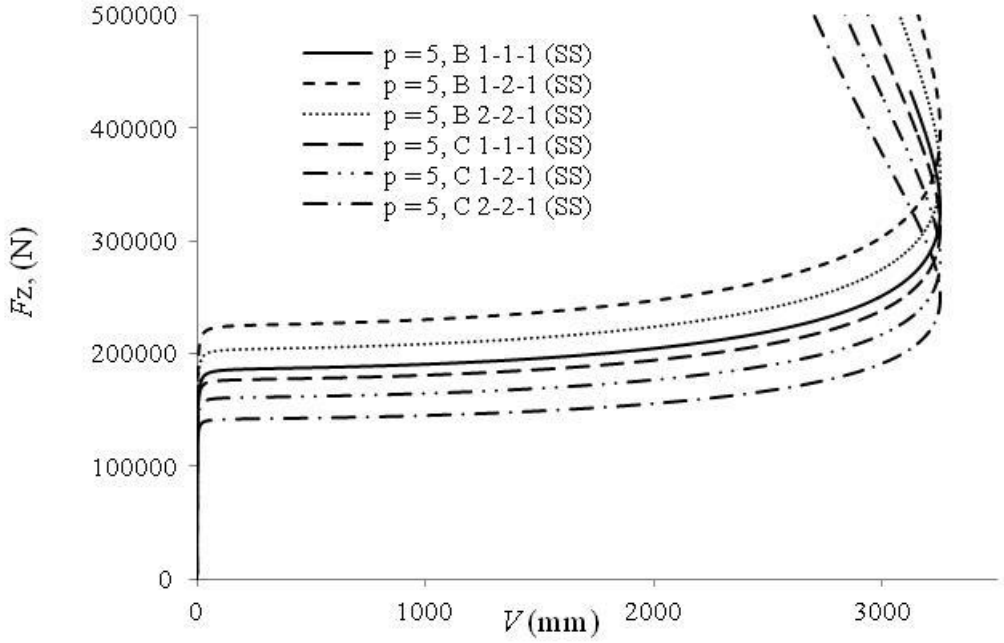

Figure 11: Load vs. displacement with the power-law index value p = 5 for simply supported boundary conditions (Types B and C).

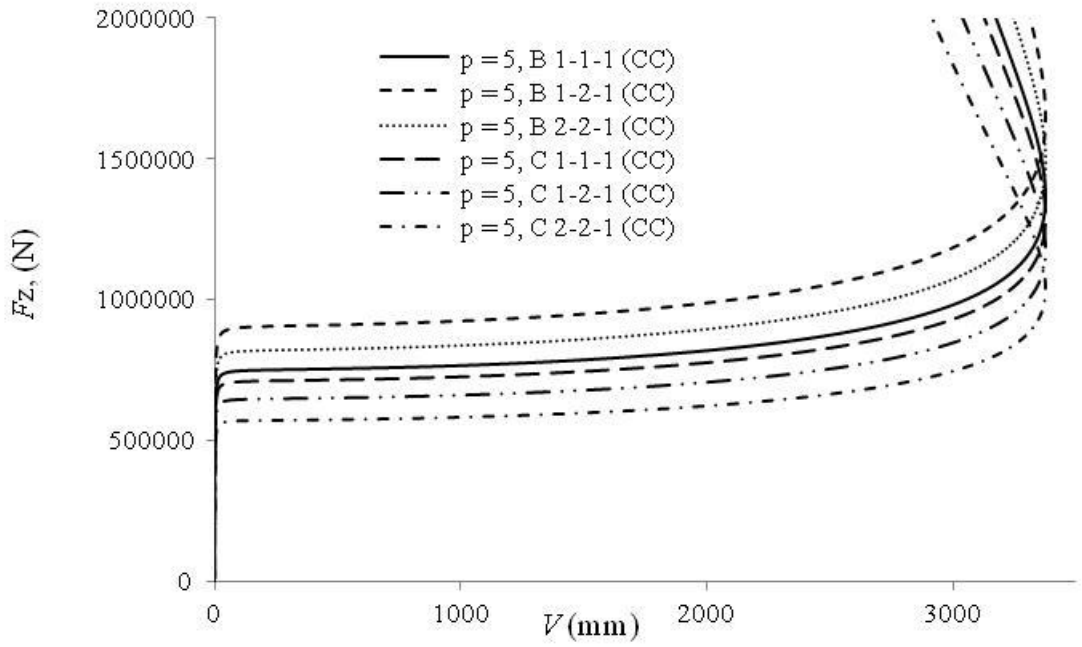

Figure 12: Load vs. displacement with the power-law index value p = 5 for clamped-clamped boundary conditions (Types B and C).

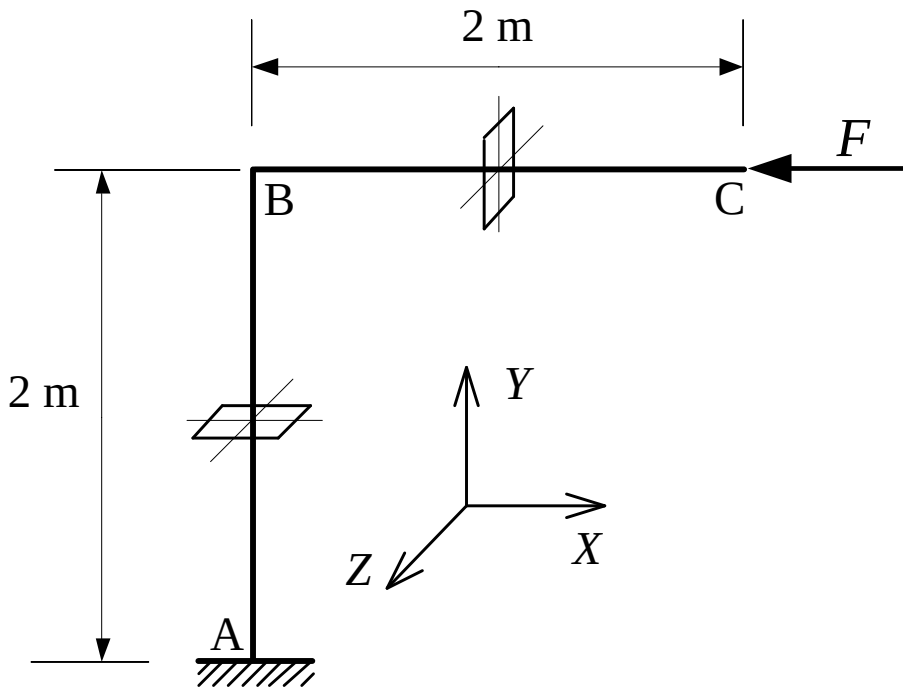

Figure 13: L-frame.

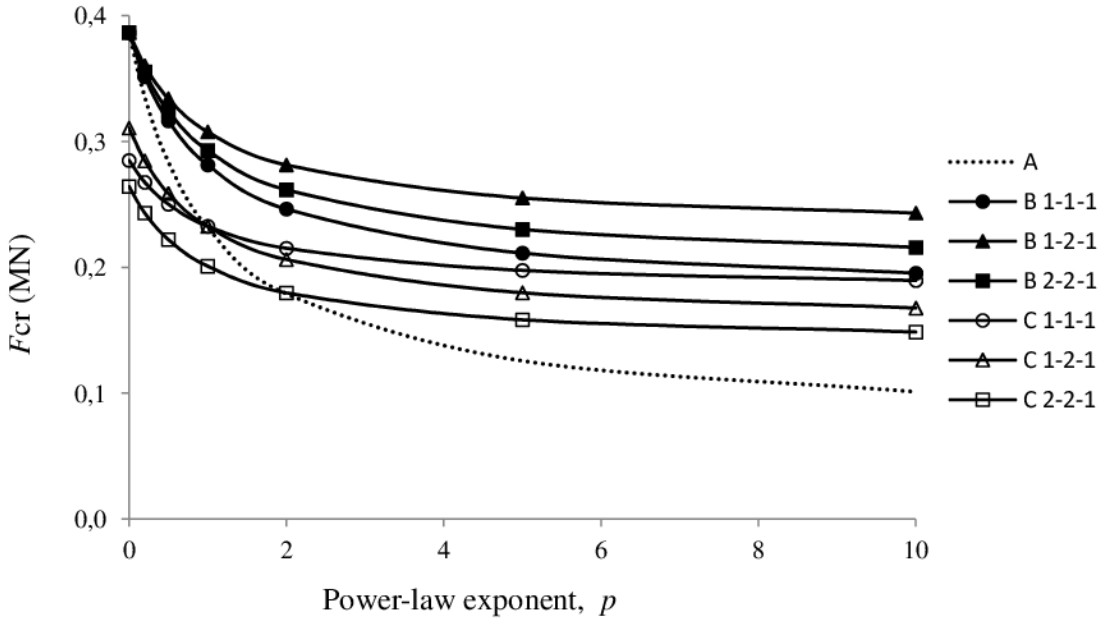

Figure 14: Critical buckling loads vs. power-law index for L-frame (Types A, B and C)

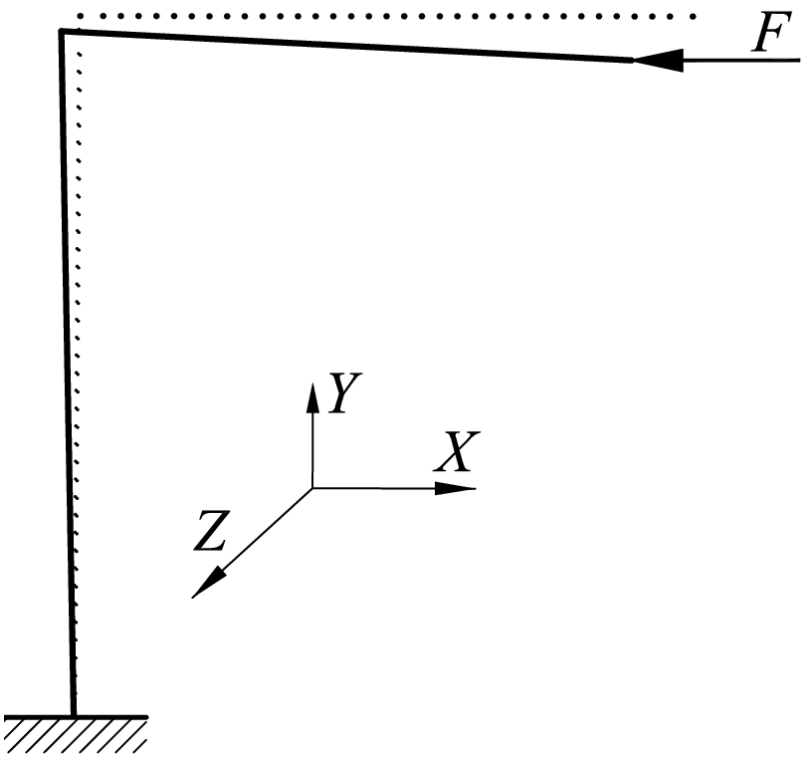

Figure 15: L-frame lateral buckling mode.

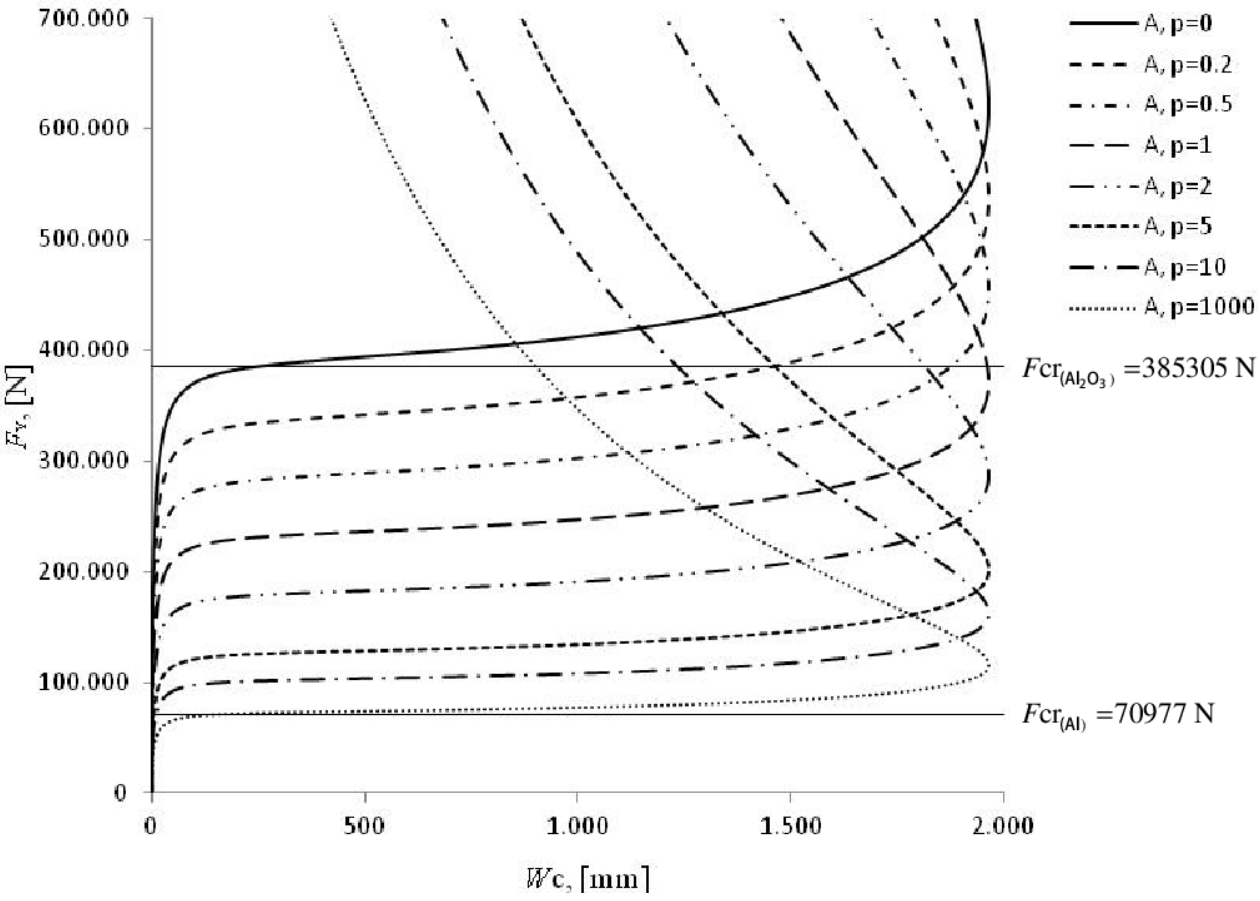

Figure 16: Load vs. displacement for L-frame (Type A) for various values of power-law index.

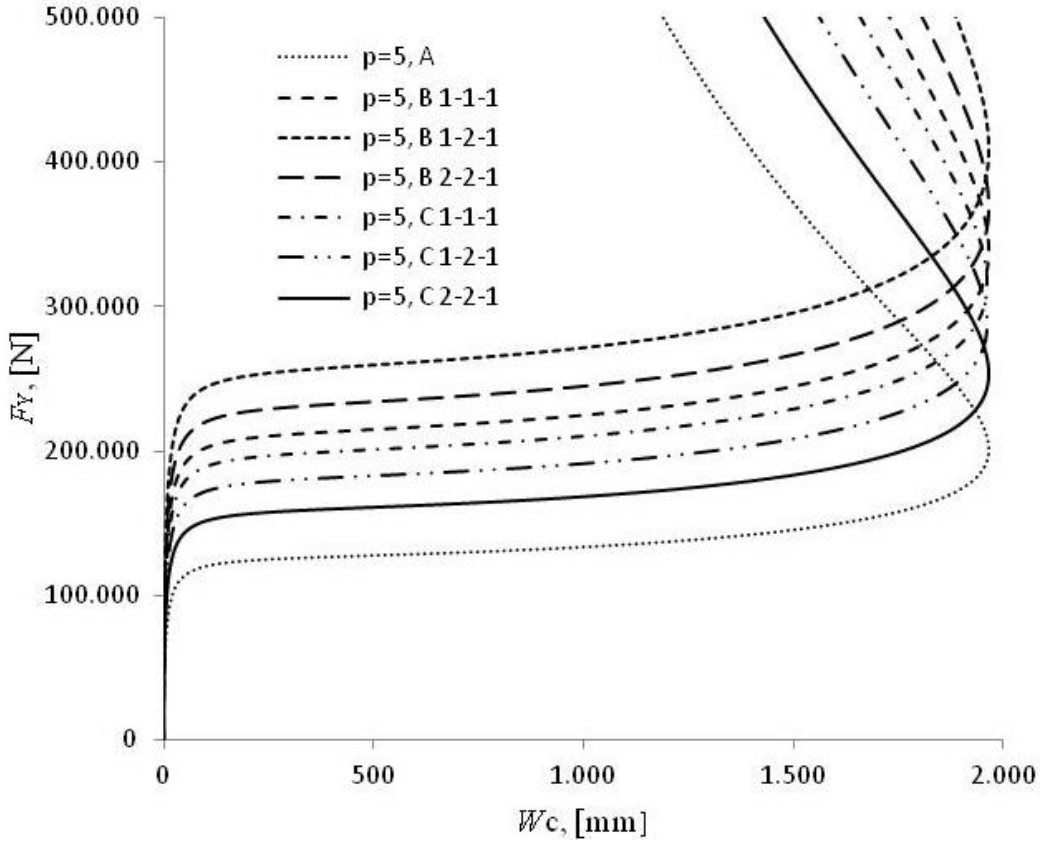

Figure 17: Load vs. displacement with the power-law index value p = 5 for L-frame (Types A, B and C).